ACS OMEGA

Open Access

http://pubs.acs.org/journal/acsodf

Article

Effect of Quorum Sensing Molecules on the Quality of Bacterial Nanocellulose Materials

Rabih E. Jabbour, Joshua S. Kang, and Hany F. Sobhi*

Cite This: *ACS Omega* 2024, 9, 20003−20011

Read Online

ACCESS | Metrics & More | Article Recommendations

ABSTRACT: Bacterial nanocellulose (BNC) biofilms, produced by various bacterial species, such as *Gluconacetobacter xylinus*, represent a highly promising multifunctional material characterized by distinctive physiochemical properties. These biofilms have demonstrated remarkable versatility as nano biomaterials, finding extensive applications across medical, defense, electronics, optics, and food industries. In contrast to plant cellulose, BNC biofilms exhibit numerous advantages, including elevated purity and crystallinity, expansive surface area, robustness, and excellent biocompatibility, making them exceptional multifunctional materials. However, their production with consistent morphological properties and their transformation into practical forms present challenges. This difficulty often arises from the heterogeneity in cell density, which is influenced by the presence of *N*-acyl-homoserine lactones (AHLs) serving as quorum sensing signaling molecules during the biosynthesis of BNC biofilms. In this study, we employed surface characterization methodologies including scanning electron microscopy, energy-dispersive spectroscopy, diffuse reflectance infrared Fourier transform spectroscopy, and atomic force microscopy to characterize BNC biofilms derived from growth media supplemented with varying concentrations of distinct *N*-acyl-homoserine lactone signaling molecules. The data obtained through these analytical techniques elucidated that the morphological properties of the BNC biofilms were influenced by the specific AHLs, signaling molecules, introduced into the growth media. These findings lay the groundwork for future exploration of leveraging synthetic biology and biomimetic methods for tailoring BNC with predetermined morphological properties.

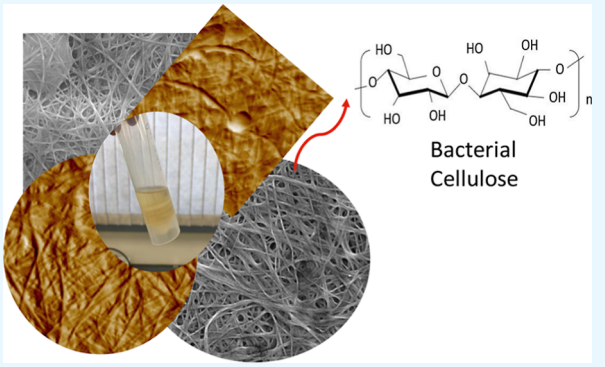

1. INTRODUCTION

Bacterial nanocellulose (BNC) is a biomaterial with promising multifunctional properties. Nanocellulose can be procured from two main sources. First, it can be extracted from plants, specifically by isolating the nanocellulose fibrils, or it can be produced by bacteria, predominantly from the genus *Gluconacetobacter*.[1,2] However, a plant-based nanocellulose material is energetically costly and laborious to manufacture. Additionally, while the small rod-like structures can be used in the production of thin films and other materials, the desired physical properties of such materials are often reduced when compared to that of the bacterial-based ones.[3]

BNC is formed at the air−media interface of active *Gluconacetobacter xylinus* cultures. BNC fibrils are synthesized from glucose units by *Acetobacter* cellulose synthase operon proteins and secreted by forming an interconnected cellulose "pellicle" around cells.[4−6] BNC pellicles are composed of long cellulose fibrils that intertwine with another and are highly free from other chemical compounds, i.e., lignin and pectin. BNC films often demonstrate a higher strength and flexibility than plant-based ones.[7] BNC can also be easily modified and functionalized through genetic engineering and/or synthetic biology approaches.[8−14] BNC materials are applied in tissue engineering applications such as regenerative medicine, where biomimetics are used as a strategy to develop scaffolds that resemble native tissues and activate self-cell regeneration.[15,16] BNC materials have excellent biocompatibility that suit them for biomedical applications such as antimicrobial treatment, wound healing,[17,18] and blood vessel replacements.[19] Moreover, the 3D-bioink printing field utilized BNC materials to form double cross-lined biomaterial films for medical field applications such as cell proliferation,[20] cartilage regeneration,[21] tissue repairs,[22] and hemostatic applications.[23] However, the BNC biofilm production process has a significant hurdle arising from the complex interplay of bacterial growth conditions and shifts in bacterial behavior during the production phase. This intricacy often renders the conversion of these BNC biofilms into a reproducible, practical, and

Received: December 15, 2023
Revised: February 26, 2024
Accepted: April 8, 2024
Published: April 24, 2024

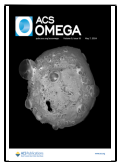

useable form a challenging endeavor.[24] Moreover, the presence of heterogeneity in cell density further compounds this process, resulting in BNC biofilms exhibiting nonuniform compositions characterized by clusters of dense regions. Despite concerted efforts to address these issues, anomalies and irregularities persist within the pellicles. Thus far, achieving precise control over critical morphological parameters such as fibrillation density, mechanical properties, and production rate remains a desirable goal in BNC biofilm production.

N-Acyl-homoserine lactones (AHLs) are vital quorum sensing (QS) molecules that enable bacterial cells to regulate growth and behavior of their community.[25] AHLs are synthesized by an AHL synthetase in the LuxI/LuxR protein family. The LuxI-type proteins are responsible for the synthesis of various AHLs and the LuxR-type protein acts as a receptor protein, initiating downstream gene expression due to the AHL binding. AHLs are utilized in bacterial QS of *Acetobacter* genius, and they play a vital role in modulating the bacterial cell density and cellulose biofilm production. AHLs affect the expression of genes related to cellulose synthesis in certain bacterial strains. The presence of excess AHL in QS could lead to the overexpression of the luxR protein, leading to an increased production of bacterial cellulose biofilms.[26−28] In Gram-negative bacteria, homoserine lactones were reported to regulate their cell density distribution and affect various functions such as motility, virulence, antibiotic biosynthesis, and biofilm formation.[29] Homoserine lactones consist of various acyl side chains of 4−14 carbon atoms and may also contain double bonds. The carbon chain of the homoserine lactones can be hydroxylated or oxidized to a carbonyl-carbon, thus resulting in quite different physicochemical properties. Homoserine lactones are the most common QS signaling molecules in Gram-negative bacteria and coordinate important temporal events, especially the formation of biofilms in nature and in human.[30,31] Based on the reported literature, we hypothesize that the manipulation of the amount of AHLs present in the bacterial growth, of bacterial cellulose forming Gram-negative bacteria, affects the morphological and physical properties of the produced BNC biofilms. Little has been known about the correlation between the bacterial cellulose production, fibril density, pellicle thickness, and the expression of different homoserine lactone QS signaling molecules. Understanding the effect of homoserine lactones, as QS signaling molecules, on the biosynthesis mechanism of BNC is vital to aid in producing the desired biofilms that can be utilized in various applications. To understand the effect of the QS signaling molecules on the production of the BNC, we performed surface characterization experiments of the produced BNC from growth media containing an exogenous amount of AHL QS signaling molecules. The surface characterization studies provided relevant information about the morphological properties of the produced BNC biofilms. Surface analysis data showed that there is a direct relationship between the different QS signaling molecules studied and the structural uniformity of the produced BNC biofilms.

2. MATERIALS AND METHODS

2.1. Bacterial Strains. The bacterial strain used to produce the nanocellulose biofilm was *G. xylinus*. The bacterial strain was obtained from ATCC as *G. xylinus* strain 10245 (Manassas, VA). The *G. xylinus* strain was cultured in Hestrin and Schramm medium (HS medium), which was composed of 2% glucose (wt/vol), 0.5% yeast extract (wt/vol), 0.5 peptone, 0.27% Na_2HPO_4 (wt/vol), and 0.15% citric acid (v/v). The stock bacterial culture was added to 10 mL of HS media in 50 mL conical tubes and was grown at 27 °C for 3−7 days depending on the amount of biofilm formation. The growth was done under a static culture in which no agitation of the culture broth was performed. Once the bacterial cellulose biofilm was formed, it was removed for further processing and characterization. All AHL standards utilized in this study were purchased from Sigma-Aldrich (Milwaukee, USA). Three AHL standards were used, namely, *N*-decanoyl-DL-homoserine lactone (DHL), *N*-dodecanoyl-L-homoserine lactone (DDHL), and *N*-(3-oxododecanoyl)-L-homoserine lactone (ODDHL). These AHL samples were dissolved in ethyl acetate and introduced to the bacterial growth media at a concentration level of 5 mg/L prior to the start of the biosynthesis phase of the bacterial biofilms in the HS media.

2.2. Cellulose Production and Purification. The bacterial cellulose biofilms were formed after 72 h of growth time on average. The formation of bacterial cellulose biofilms occurred in static culture; cells were grown in a 50 mL conical tube containing 10 mL of HS medium at 27 °C for 3−7 days. The cellulose pellicles were then isolated and purified by treating them with 0.5% NaOH at 100 °C for 1 h, followed by extensive washing with Milli-Q-H_2O to remove the excess NaOH solution and reduce the pH. The pH of the pellicle was checked periodically during washing step and was maintained at 4−5. Following the water washing step, the pellicles were dried at 30 °C for 24 h and then weighed on an analytical balance. The obtained mass was normalized to include the culture volume used to compare the pellicles' yield from the addition of different homoserine lactones. Cleaned but not processed pellicles were kept in a 0.1 M sodium azide solution under ambient conditions.

2.3. Analysis of the Surface Morphology of BNC Biofilms by SEM and AFM Techniques. For the analysis of the physical and chemical characteristics of BNC films, various techniques and machines such as scanning electron microscopy (SEM), atomic force microscopy (AFM), TEM, Fourier-transform infrared (FTIR), HPLC, DLS, tensile test machine, thickness test machine, XRD, XRF, and TGA are employed. To examine the surface morphology of the films, SEM, TEM, and AFM machines are primarily used.[14,32−34] In this research, SEM (JSM 7100F, Jeol. co) and AFM (NT-MDT co.) machines are utilized to characterize the surface morphology properties of the bacterial cellulose films produced for control, DHL, DDHL, and ODDHL samples. To obtain the images, the beam energy of the SEM instrument was set to 5 keV. Prior to acquisition of images, the bacterial cellulose pellicles were coated with ∼>2 nm of gold by sputtering to reduce the charging and beam damage effects from the electron beam. A piece of each BNC film was fixed on a SEM standard holder using carbon tape. Energy-dispersive spectroscopy (EDS, JED-2300) was utilized to determine the elemental content of the analyzed bacterial cellulose pellicles. To obtain the AFM topology images, a piece of the film was fixed on an AFM holder by using a carbon tape and was taken in semicontact mode using a silicon cantilever. The topography images were gained in 256 × 256 scan points at a scan speed of 1 Hz. In addition, the Mag mode images, one of the image functions in NT-MDT software, which is due to the amplitude of oscillation of the cantilever, were supported with the

https://doi.org/10.1021/acsomega.3c10053
ACS Omega 2024, 9, 20003−20011

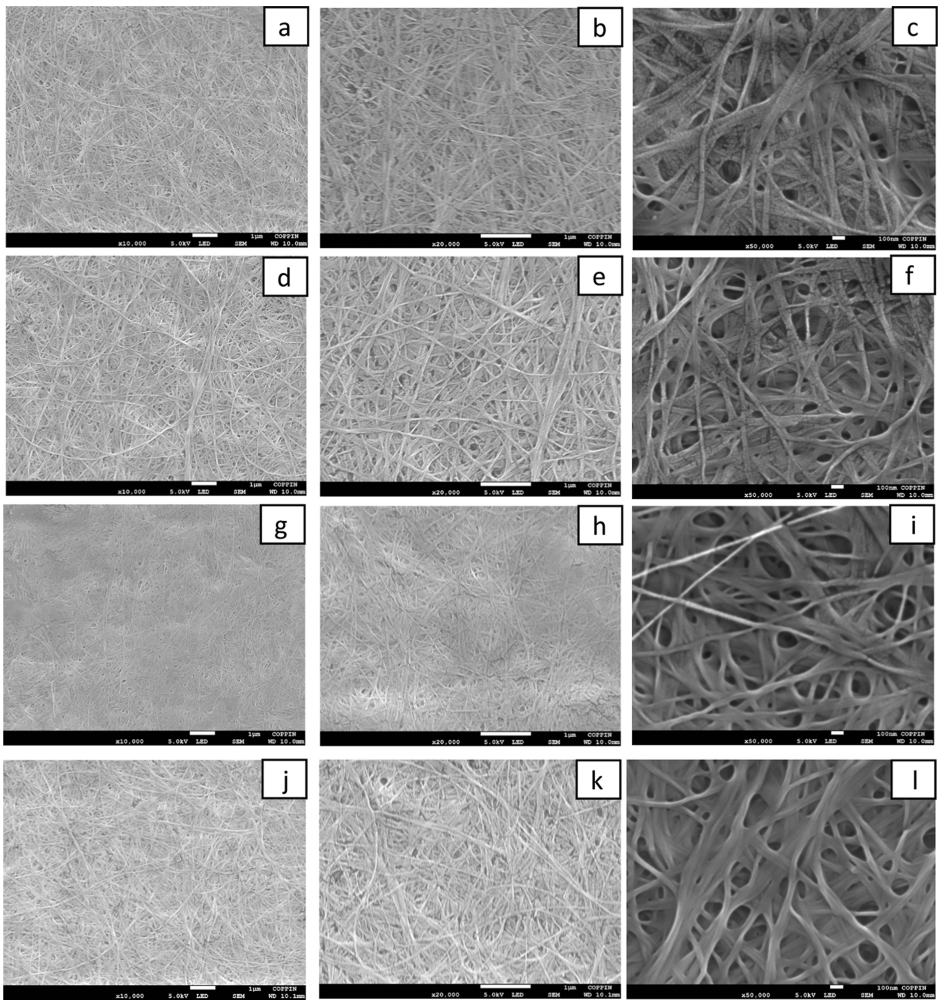

Figure 1. Morphological images for various homoserine lactone molecules: (a) ×10k, (b) ×20k, and (c) ×50k for control; (d) ×10k, (e) ×20k, and (f) ×50k for DHL; (g) ×10k, (h) ×20k, and (i) ×50k for DDHL; and (j) ×10k, (k) ×20k, and (l) ×50k for ODDHL.

topography images. The AFM images were acquired in various scan regions of the deposited bacterial cellulose biofilms.

2.4. In Situ Diffuse Reflectance Infrared Fourier Transform Spectroscopy of BNC Biofilms. Individual biosynthesized cellulose samples were cut using a stainless steel "fly-typing" scissor from a larger film to fit snuggly into ceramic cups (6.0 mm OD, 4.0 mm height, 4.7 mm ID, 2.0 mm depth). The cut samples were gently pressed into a ceramic cup with a sample loading tool. The cellulose-film-containing ceramic cups were placed onto a macro-diffuse reflectance infrared Fourier transform spectroscopy (DRIFTS) cell holder. The macro-DRIFTS cell holder was then inserted in a Harrick Scientific Products Inc. Praying Mantis Diffuse Reflection Accessory (Pleasantville, New York 10570 USA) located within the chamber compartment of a Thermo Scientific Nicolet Avatar 380 FTIR (Waltham, MA 02451 USA) outfitted with an MCT/A detector and a KBr beam splitter. The optics bench and accessory were purged by using a FTIR Purge Gas Generator. Diamond dust (4000 grit, annealed to 350 °C for 90 min) was used as a baseline spectrum for the Kubelka−Munk single beam spectral scans.

Background spectra were collected with 1024 scans per spectrum. Sample spectra were collected in the following manner: 128 scans were collected with a collection time of 346.40 s. Instrumental resolution was kept at 2.000 cm^{-1} with levels of zero filling kept at zero. For each scan, there are 33,056 points with 32,768 FFT points. The HeNe laser frequency was 15,798.25 cm^{-1} (632.97 nm), and the interferogram peak position was 16,384 cm^{-1}. The Happ−Genzel anodization function and the Mertz phase correction were used for the FTIR signaling processing. The data represent 3475 points between 649.9254 and 3999.8381 cm^{-1}, with a spectral data spacing of 0.964281 cm^{-1}. The optical velocity was held at 0.4747 cm/s with an aperture of 100.00% and a sample gain of 2.0. The high-pass filter and low-pass filter were set to 20.0 and 11,000.0 Hz, respectively.

3. RESULTS AND DISCUSSION

The SEM technique provides useful morphological information about the potential 2D-spatial variation to compare the different bacterial cellulose fibrils produced from the presence of different AHLs in the growth media of *G. xylinus*. The SEM image analysis was focused on determining any potential changes of the BNC fibrils in terms of their diameter and the structural changes after the addition of the AHL signaling molecules. The SEM images were acquired at an acceleration voltage of 5 keV at various magnifications. It was cumbersome to get a good resolution image in high magnification because the fibrils start to crack and burn out at high beam energies. Four pellicles were analyzed, including a control pellicle

https://doi.org/10.1021/acsomega.3c10053
ACS Omega 2024, 9, 20003−20011

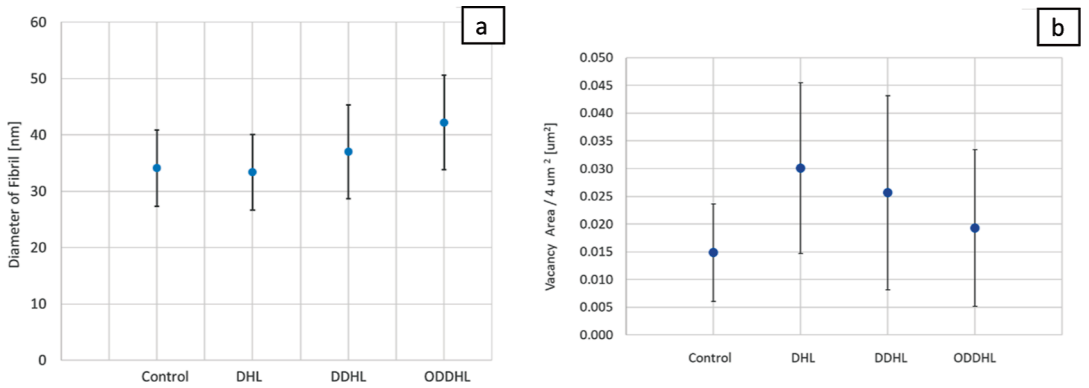

Figure 2. Analysis for control, DHL, DDHL, and ODDHL pellicles: (a) diameter of the four different pellicles and (b) vacancy area of the four different pellicles.

1(f).

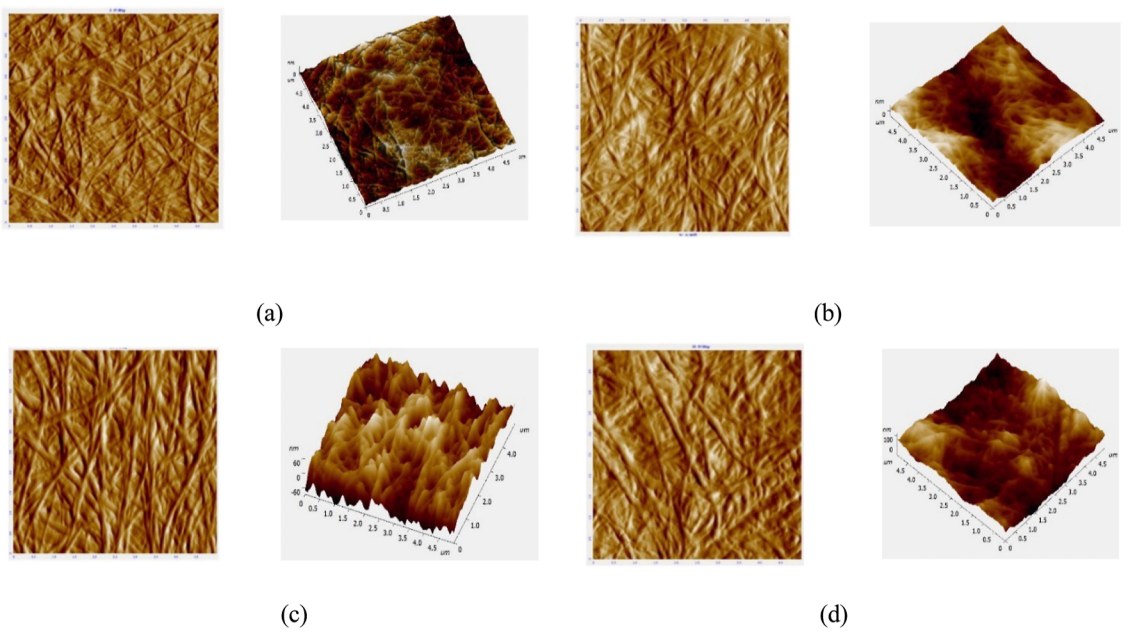

Figure 3. AFM analyses of the BNC samples: (a) AFM image in Mag mode and 3D topography for control. (b) AFM image in Mag mode and 3D topography for DHL. (c) AFM image in Mag mode and 3D topography for DDHL. (d) AFM image in Mag mode and 3D topography for ODDHL.

without AHL signaling molecules. Figure 1 shows a comparison between the control-BNC, the DHL-BNC fibers, the DDHL-BNC, and the ODDHL-BNC fibrils on the three different magnification settings, i.e., ×10K, ×20K, and ×50K. There were variabilities in the structure and diameter of the pellicles produced in the presence of various AHLs as compared to that of the control ones. After SEM images were taken from the four pellicles, the diameter of the fibrils and the vacancy area in the pellicles were measured. Though the average value of each fibril is in the standard deviation value of each fibril in the four BNCs, as shown in Figure 2a, it was observed that the AHL molecules influence the diameter of the fibrils during the growth. The vacancy area was calculated from the 4 μm^2 SEM image of each pellicle (Figure 2b) to compare the surface morphology of the pellicle. In the DDHL-BNC, the fibrils are not well formed, but an amorphous shape and a structural deformity are observed as compared with the fibrils in the control, as shown in Figure 1a−c,g−i. It could be the result of the DDHL molecules disrupting the formation mechanism of the cellulose fibrils. Overall, the DDHL-BNC pellicle shows high porosity as compared with that of the control-BNC pellicle.

Comparing the SEM images of the control and ODDHL-BNC samples showed that the fibrils produced in the presence of ODDHL are well formed and tightly packed with a high density of BNC fibers in the field of view as compared to that of the control SEM image. In addition, the ODDHL fibrils have more aggregations than the control ones, as shown in Figure 1l. Also, the diameter of the ODDHL fibrils was found to be the highest among the four BNC fibrils based on the calculated result from the SEM images, which could be due to more aggregation patterns in the ODDHL-produced fibrils. The ODDHL-BNC SEM images also showed a well-formed and less structural deformity when compared with that of DDHL-BNC. The ODDHL-BNC fibrils showed less porosity and higher fiber density as compared to that of DHL and DDHL pellicles, as shown in Figure 2b.

https://doi.org/10.1021/acsomega.3c10053
ACS Omega 2024, 9, 20003−20011

Figure 1a−f shows an SEM-based comparison between the control-BNC and the DHL-BNC fibrils. The DHL-BNC SEM image shows that the fibrils are well formed and tightly packed with a high density of BNC fibers in the field of view. However, the aggregated fibrils and the many small vacancies are observed in Figures 1f and 2b. The DHL-BNC fibrils have a similar morphology to that of the ODDHL-BNC ones, except that the former are more uniform and have less variability in the fiber morphological properties such as the width, the thickness, and the distribution of their fibrils. The DHL-BNC SEM image showed a well-formed and more structural uniformity compared with that of the ODDHL-BNC ones. Also, the average diameter of the BNC fibers for the control-BNC and DDHL-BNC samples was measured using the SEM analysis software. These measurements showed that the average diameter of the ODDHL-BNC (42 nm) sample was slightly larger than that of the control-BNC (34 nm) sample.

Comparing the SEM data for all AHLs used in the production of the BNC fibrils in these experiments showed that their presence affected the formation and the morphological properties of the BNC pellicles. The AHL effect on the morphological properties of the BNC pellicles varied based on the molecule used. The DHL-BNC and ODDHL pellicles have a good morphological property, while the DDHL pellicles have an amorphous shape as compared to that of the control. One common effect among the three used AHLs was the enlargement of the fiber average diameter as compared to that of the control-BNC samples, as shown in Figure 2a. The average diameter of the ODDHL-BNC (42 nm) sample was larger than that of the control-BNC (34 nm) sample. While this explanation is based on experimental morphological data, further genomic and mechanistic investigations of the factors leading to such enlargement in the pellicle's diameter will be biologically informative. These proposed experiments will address, on the molecular level, the impact of genetic materials responsible for the secretion of AHLs and how such factors when manipulated can impact the formation of BNC pellicles. Overall, SEM data showed that AHLs play a critical role in affecting the morphology of the BNC pellicles, and using different AHL molecules showed that the signaling molecules affected the mechanism of formation of the pellicles to various degrees and resulted in unique BNC pellicles that can be utilized for various applications.

Figure 3 shows the AFM data collected in the Mag mode and the topography of each cellulose pellicle. The Mag image is the amplitude of the oscillation of the cantilever. The two AFM images clearly show the structure of the cellulose sample, and the images allow us to measure the width of the cellulose fibers. The images were obtained in various scan regions. The images shown in Figure 3 are obtained in 5 μm × 5 μm areas from the 256 × 256 scan points. Details of the surface structure of bacterial cellulose fibers at the nanometer scale were observed in the topology and Mag mode images. Based on the AFM topography images, the roughness was calculated (Figure 4). In the roughness measurement, the DHL-BNC fibrils showed a little high roughness value compared to that of the control and DDHL BNCs, but the values were in the range of the error bar and some aggregated fibril structures, and the number of vacancies in the scan area caused the high roughness value. Figure 4 shows the comparison of the calculated roughness with the roughness value of the ODDHL-BNC fibril having the highest value among the four BNC fibrils. The roughness is dependent on the number and size of

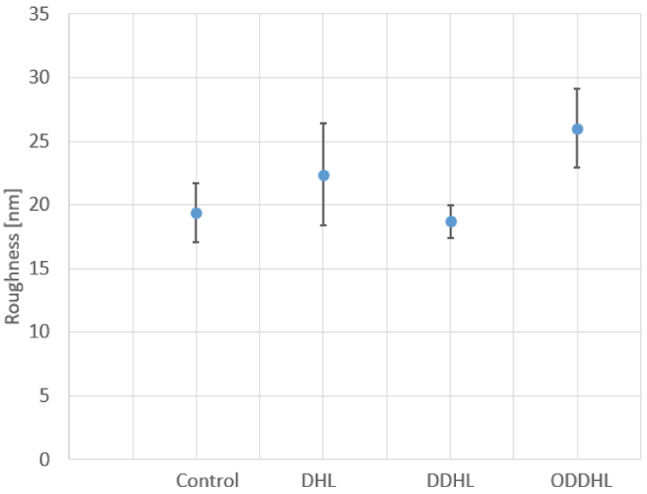

Figure 4. Roughness measurements of the BNC samples using AFM.

atypical vacancies and the diameter of fibrils. Among the studied fibrils, the ODDHL-BNC fibrils have the highest diameter with a wide standard deviation value due to the aggregated fibrils; see Figures 3d and 1l. While the DHL-BNC fibrils have the smallest diameter among all the studied samples, they had a higher roughness value with a wide standard deviation than that of the control and DDHL-BNC. It is noteworthy that the average roughness of the control and DDHL samples was in the range of the standard deviation of the DHL-BNC sample. The high roughness of the DHL-BNC sample is due to more atypical vacancies than that of the control and DDHL-BNC, as shown in Figure 1f.

3.1. Effect of the Type of Homoserine Lactones (AHLs) on the Uniformity of BNC Biofilms. The DRIFTS technique was used to determine the structural differences of the BNC fibrils. DRIFTS provided useful information on the changes in the crystalline and amorphous structures of the cellulose and on the uniformity of the BNC film. Samples were collected from three different AHL-BNC fibrils, namely, the control-BNC, ODDHL-BNC, and DHL-BNC samples. These samples were formed in a disc shape. Each disc-shaped sample was ground to form a homogeneous powder and analyzed by the DRIFTS technique. These AHL samples were selected from different regions of the bacterial cellulose biofilm disc, mainly the peripheral and center areas. The DRIFTS results for the three samples are shown in Figure 5. In the DRIFTS result, there are two important regions that are considered to determine structural properties, namely, the hydroxyl (O−H) region between 4000 and 2500 cm^{-1} and the fingerprint region ranging between 1600 and 600 cm^{-1}. The relevant variation in the hydroxyl region is in its bandwidth range. The variation in the hydroxyl region bandwidth represents structural variation of the film, for example, the wider the hydroxyl region, the more amorphous structure the film is, and the narrower the hydroxyl band region, the more crystalline structure and uniform the film is.[35,36] Comparing the O−H stretching bands of the control-BNC and ODDHL-BNC samples showed that the control-BNC fibrils are not as uniform as that of the ODDHL_BNC biofilms. The latter fibrils had a narrower hydroxyl stretching band than the control-BNC. Moreover, the ODDHL-BNC fibrils were more uniform because of smaller variation in the hydroxyl stretching band. These DRIFTS spectra were reproducible from the three samples of ODDHL-BNC, which indicate that there is a uniformity in the structure

https://doi.org/10.1021/acsomega.3c10053
ACS Omega 2024, 9, 20003−20011

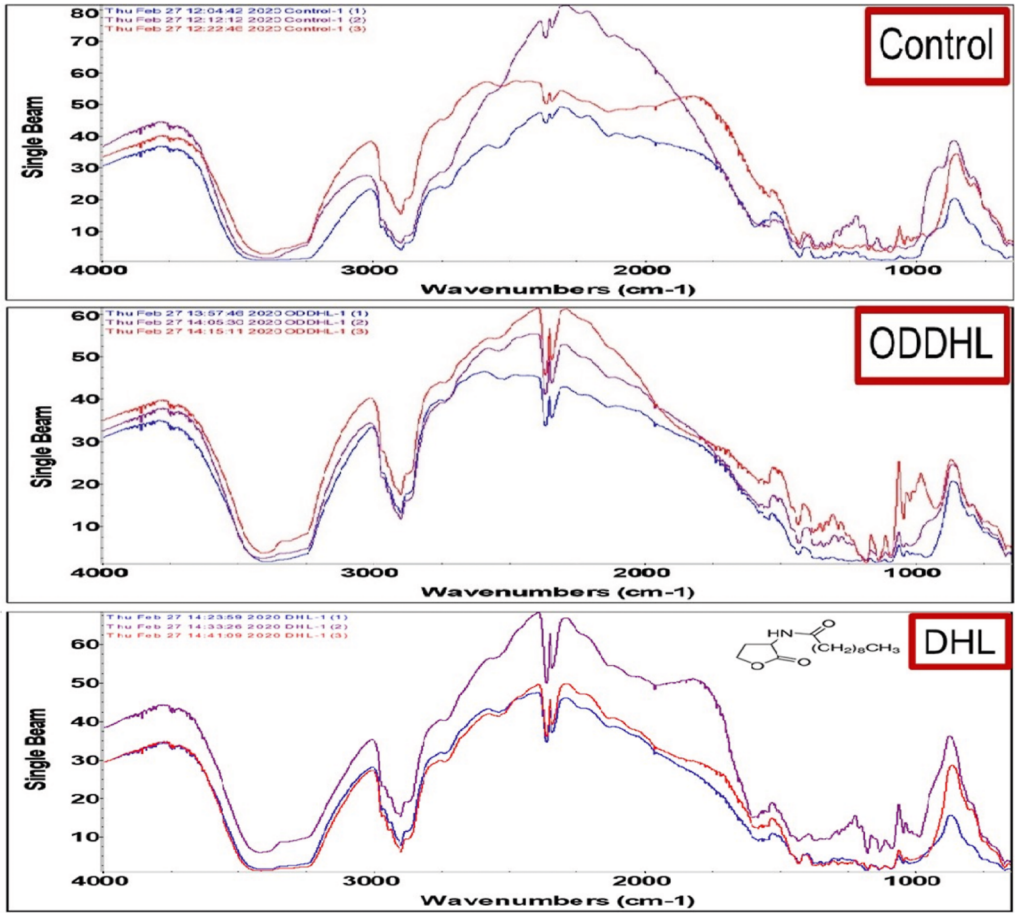

Figure 5. DRIFTS analyses of control, ODDHL, and DHL BNC samples collected from different regions of a disc-shaped BNC film: (top) three control-BNC samples, (middle) three ODDHL-BNC samples, and (bottom) three DHL-BNC samples.

of the BNC fibril across the whole area more than that of the control-BNC fibrils. The bandwidth in the ODDHL-BNC fibril is narrower than that in the control-BNC, which suggests that the predominant intermolecular hydrogen bonds exhibit an isotropic behavior more than that of control-BNC fibrils. Moreover, the narrower O−H absorption band in ODDHL-BNC is potentially indicative of more crystalline structures as compared to that of the control-BNC sample.[35]

In the fingerprint region, the ODDHL-BNC biofilms showed significant inter- and intrastructural differences when compared to the control-BNC ones. The ODDHL-BNC fibrils had fewer variabilities in this fingerprint region than that of the control-BNC fibrils. The C−O−C stretching band absorption at 1050 cm^{-1} is more predominant in the ODDHL-BNC biofilm than that in the control-BNC biofilms, which indicates more crystalline structure properties as the absorption increases. Also, in the fingerprint region, there is a clear difference in the spectral reproducibility observed with the control-BNC fibrils. This is another indication of the clear difference in the uniformity of the BNC biofilms in the control-BNC sample. This variation in the fingerprint region is not observed with the spectral signature of ODDHL-BNC, where the differences in the spectral signature across the three analyzed samples are in the absorption intensity rather than the number of peaks. As such, we can conclude that the ODDHL-BNC biofilm is more uniform than that of the control-BNC one.

These DRIFTS data for the characterization of the ODDHL-BNC samples agree with their corresponding SEM images, which showed the ODDHL-BNC fibrils to be more uniform with less variation in their thickness, fiber size, and layer distribution. Also, the shape of the peak at 750 cm^{-1} along with the shoulder grooves at 710 cm^{-1} in both DRIFTS spectra enabled us to characterize the crystalline structure of the two BNC films. In this case, the control-BNC has more shoulders and roughness in the region between 750 and 700 cm^{-1}, which is indicative of an amorphous structure in a monoclinic arrangement.[37] It was worth mentioning that the water capacity of the ODDHL-fibrils was higher than that of the control-BNC. This was observed during the washing step of the biofilms, where the wet bacterial cellulose membranes from all cultured samples were weighted before and after drying. The weight of wet ODDHL-BNC fibrils was 1.8 times more than that of the control-BNC ones.

The DRIFTS results for the DHL-BNC samples showed a highly reproducible hydroxyl (O−H) region between 4000 and 2500 cm^{-1} and a fingerprint region between 1600 and 600 cm^{-1}. This reproducible hydroxyl stretching band region observed with the DHL-BNC fibril indicates that the DHL-BNC film is more uniform than that of the control-BNC film. The hydroxyl region bandwidth in DHL-BNC is narrower than that in the control-BNC, which suggests that the predominant intermolecular hydrogen bonds in the DHL-BNC film exhibit an isotropic behavior more than that in the control-BNC film. The narrower absorption bands observed for the DHL-BNC

https://doi.org/10.1021/acsomega.3c10053
ACS Omega 2024, 9, 20003−20011

film are indicative of more crystalline structures as compared to that of the control-BNC sample.

In the fingerprint region, similar fingerprint peaks were observed when comparing the DHL-BNC sample to the control-BNC one. The C−O−C stretching band absorption at 1050 cm^{-1} has a slightly higher intensity in DHL-BNC than that in control-BNC spectra, which indicates that more crystalline structure properties are observed in the DHL-BNC sample due to an increase in absorption intensity. Also, in the fingerprint region, there is a clear difference in the spectral reproducibility observed with the control-BNC fibrils and less variation in the shoulder peaks, which indicate smoothness of molecular distribution or more uniform molecular densities in the DHL-BNC fibril. This spectral signature in 750 cm^{-1} for the control-BNC samples with more shoulder peaks is indicative of differences in the uniformity of the BNC film produced in the control growth conditions. This variation in the fingerprint region is not observed with DHL-BNC. As such, we can conclude that the DHL-BNC film is more uniform than that of the control-BNC one. This agrees with the SEM data that showed the DHL-BNC fibrils to be more uniform with less variation in its thickness and fiber size and layer distribution. In this case, the control-BNC has more shoulders and roughness in the region between 750 and 700 cm^{-1}, which is indicative of a crystalline structure in a monoclinic arrangement.

Overall, DRIFTS data showed that the DHL-BNC sample is more uniform than that of ODDHL and that this observation is supported by the SEM data. These DRIFTS results are important because they indicate that the AHL signaling activities can improve the morphological properties and structures of the BNC fibrils, which result in the synthesis of more reproducible biofilms with different morphological properties than the control-BNC biofilms.

The EDS technique was used to measure the elemental composition of the studied bacterial cellulose samples. Figure 6

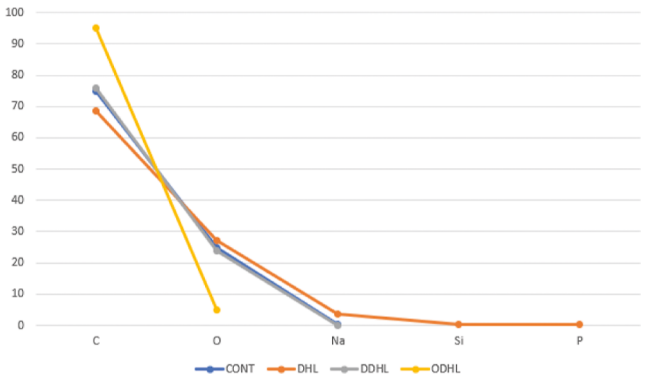

Figure 6. Element analysis by EDS for control, DHL, DDHL, and ODDH. This figure shows the variance in the elemental composition of the four analyzed bacterial samples that have different homoserine lactones.

presents the EDS results that showed that carbon and oxygen were detected as the common and dominant elements in all analyzed samples. Sodium, silicon, and phosphorus were observed to a lesser extent than that of carbon and oxygen, and their presence could be attributed to the sample fabrication process in terms of impurities in the growth media. Moreover, the EDS results showed that using equal mass of nanocellulose samples, the ratio of carbon to oxygen was highest for the ODDHL-BNC film and lowest for the DHL-BNC biofilm. This change in the C/O ratio among the analyzed biofilms could be attributed to variation in the biofilm's density as a factor of the type of the homoserine lactones used.

4. CONCLUSIONS

The utilization of a combination of biological methods and surface characterization techniques confirmed the impact of auxiliary AHLs, present in growth media as QS signaling molecules, on the morphological properties of the BNC biofilms. The results showed that the morphology of the produced BNC biofilms can be controlled through the manipulation of the type of the studied QS signaling molecules in terms of the elements and the fibril structure such as aggregated fibrils, the number of vacancies in the nanocellulose pellicle, and the uniformity of the biofilm. Utilization of auxiliary DDHL in growth media would result in amorphous fibrils as those produced in the presence of DHL or ODDHL. Moreover, production of aggregate biofilms could be accomplished by adding an extra amount of ODDHL as compared to the other studied QS molecules. Better understanding of the impact of AHL QS molecules on the physical properties of BC biofilms will lead to the production of customized biofilm mechanical properties for specific biomedical or industrial requirements. Moreover, controlling BC biofilm production could lead to optimizing its porosity and permeability for filtration applications. Manipulating the QS mechanism will lead to design tailored biofilms, enabling advancement in biomedical areas such as wound healing, tissue engineering, and other biofabrication applications. Finally, applying more in-depth synthetic biology approaches for a comprehensive understanding of AHL-mediated regulations in BC biofilms will have practical implications for various biotechnological processes. Such molecular level knowledge will be leveraged to optimize BNC biofilm production for applications in various industries.

AUTHOR INFORMATION

Corresponding Author

Hany F. Sobhi − *Center for Organic Synthesis, Department of Natural Sciences, Coppin State University, Baltimore, Maryland 21216, United States;* orcid.org/0009-0007-4278-3524; Email: hsobhi@coppin.edu

Authors

Rabih E. Jabbour − *U.S. Army Edgewood Chemical Biological Center, Research & Technology Directorate, Aberdeen, Maryland 21010, United States*

Joshua S. Kang − *Center for Organic Synthesis, Department of Natural Sciences, Coppin State University, Baltimore, Maryland 21216, United States*

Complete contact information is available at: https://pubs.acs.org/10.1021/acsomega.3c10053

Author Contributions

Funding acquisition and conceptualization, taking DRIFTS data, and reviewing—Rabih E. Jabbour and Hany F. Sobhi, taking SEM and AFM data, analyzing, reviewing, and editing—Joshua S. Kang; all authors have read and agreed to the published version of the manuscript.

https://doi.org/10.1021/acsomega.3c10053
ACS Omega 2024, 9, 20003−20011

Notes

The authors declare no competing financial interest.

■ ACKNOWLEDGMENTS

This work was supported by the University System of Maryland USM-(Wilson H. Elkins Dr. Sobhi's Professorship award); the authors are grateful to Alex Balboa, Erik Emmons, and Ashish Tripathi for SEM and AFM data analyses.

■ REFERENCES

(1) Yuan, J. C.; Huang, R.; Jiang, L. Y.; Liu, G. D.; Liu, P. D.; Xu, W. R. Facile production of cellulose nanofibers from raw elephant grass by an aluminum chloride-enhanced acidic deep eutectic solvent. *Int. J. Biol. Macromol.* **2023**, *246* (15), 125687.

(2) Trache, D.; Tarchoun, A. F.; Derradji, M.; Hamidon, T. S.; Masruchin, N.; Brosse, N.; Hussin, M. H. Nanocellulose: From Fundamentals to Advanced Applications. *Front. Chem.* **2020**, *8*, 392.

(3) Thomas, B.; Raj, M. C.; Athira, K. B.; Rubiyah, M. H.; Joy, J.; Moores, A.; Drisko, G. L.; Sanchez, C. Nanocellulose, a Versatile Green Platform: From Biosources to Materials and Their Applications. *Chem. Rev.* **2018**, *118* (24), 11575−11625.

(4) Lee, K. Y.; Buldum, G.; Mantalaris, A.; Bismarck, A. More than meets the eye in bacterial cellulose: Biosynthesis, bioprocessing, and applications in advanced fiber composites. *Macromol. Biosci.* **2014**, *14* (1), 10−32.

(5) Rognoli, V.; Bianchini, M.; Maffei, S.; Karana, E. DIY materials. *Mater. Des.* **2015**, *86*, 692−702.

(6) Buldum, G.; Bismarck, A.; Mantalaris, A. Recombinant biosynthesis of bacterial cellulose in genetically modified Escherichia coli. *Bioprocess Biosyst. Eng.* **2018**, *41*, 265−279.

(7) Mangayil, R.; Rajala, S.; Pammo, A.; Sarlin, E.; Luo, J.; Santala, V.; Karp, M.; Tuukkanen, S. Engineering and Characterization of Bacterial Nanocellulose Films as Low Cost and Flexible Sensor Material. *ACS Appl. Mater. Interfaces* **2017**, *9* (22), 19048−19056.

(8) Zhong, C.; Gurry, T.; Cheng, A. A.; Downey, J.; Deng, Z.; Stultz, C. M.; Lu, T. K. Strong underwater adhesives made by self-assembling multiprotein nanofibres. *Nat. Nanotechnol.* **2014**, *9* (10), 858−866.

(9) Chen, A. Y.; Deng, Z.; Billings, A. N.; Seker, U. O. S.; Lu, M.; Citorik, R. J.; Zakeri, B.; Lu, T. K. Synthesis and patterning of tunable multiscale materials with engineered cells. *Nat. Mater.* **2014**, *13* (5), 515−523.

(10) Vikas, Y.; Paniliatis, B. J.; Shi, H.; Lee, K.; Cebe, P.; Kaplan, D. L. Novel in vivo-degradable cellulose-chitin copolymer from metabolically engineered Gluconacetobacter xylinus. *Appl. Environ. Microbiol.* **2010**, *76* (18), 6257−6265.

(11) Mohite, B. V.; Patil, S. V. Physical, structural, mechanical, and thermal characterization of bacterial cellulose by G. hansenii NCIM 2529. *Carbohydr. Polym.* **2014**, *106*, 132−141.

(12) Hsieh, Y. C.; Yano, H.; Nogi, M.; Eichhorn, S. J. An estimation of the Young's modulus of bacterial cellulose filaments. *Cellulose* **2008**, *15* (4), 507−513.

(13) Barja, F. Bacterial nanocellulose production and biomedical applications. *J. Biomed. Res.* **2021**, *35* (4), 310−317.

(14) Murugarren, N.; Roig-Sanchez, S.; Antón-Sales, I.; Malandain, N.; Xu, K.; Solano, E.; Reparaz, J. S.; Laromaine, A. Highly Aligned Bacterial Nanocellulose Films Obtained During Static Biosynthesis in a Reproducible and Straightforward Approach. *Adv. Sci.* **2022**, *9*, 2201947.

(15) Cañas-Gutiérrez, A.; Toro, L.; Fornaguera, C.; Borrós, S.; Osorio, M.; Castro-Herazo, C.; Arboleda-Toro, D. Biomineralization in Three-Dimensional Scaffolds Based on Bacterial Nanocellulose for Bone Tissue Engineering: Feature Characterization and Stem Cell Differentiation. *Polymers* **2023**, *15*, 2012.

(16) Choi, S. M.; Rao, K. M.; Zo, S. M.; Shin, E. J.; Han, S. S. Bacterial Cellulose and Its Applications. *Polymers* **2022**, *14*, 1080.

(17) Gonçalves, I. S.; Lima, L. R.; Berretta, A. A.; Amorim, N. A.; Pratavieira, S.; Corrêa, T. Q.; Nogueira, F. A. R.; Barud, H. S. Antimicrobial formulation of a bacterial nanocellulose/propolis-containing photosensitizer for biomedical applications. *Polymers* **2023**, *15*, 987.

(18) Yuan, H.; Chen, L.; Hong, F. F. A biodegradable antibacterial nanocomposite based on oxidized bacterial nanocellulose for rapid hemostasis and wound healing. *ACS Appl. Mater. Interfaces* **2019**, *12*, 3382−3392.

(19) Hu, G.; Chen, L.; Zhao, S.; Hong, F. F. Mercerization of tubular bacterial nanocellulose for control of the size and performance of small-caliber vascular grafts. *Chem. Eng. J.* **2022**, *428*, 131104.

(20) Zhang, S.; Chen, X.; Shan, M.; Hao, Z.; Zhang, X.; Meng, L.; Zhai, Z.; Zhang, L.; Liu, X.; Wang, X. Convergence of 3D Bioprinting and Nanotechnology in Tissue Engineering Scaffolds. *Biomimetics* **2023**, *8*, 94.

(21) Apelgren, P.; Karabulut, E.; Amoroso, M.; Mantas, A.; Martínez Ávila, H.; Kölby, L.; Kondo, T.; Toriz, G.; Gatenholm, P. In vivo human cartilage formation in three-dimensional bioprinted constructs with a novel bacterial nanocellulose bioink. *ACS Biomater. Sci. Eng.* **2019**, *5*, 2482−2490.

(22) Sämfors, S.; Karlsson, K.; Sundberg, J.; Markstedt, K.; Gatenholm, P. Biofabrication of bacterial nanocellulose scaffolds with complex vascular structure. *Biofabrication* **2019**, *11*, 045010.

(23) Roberts, E. L.; Abdollahi, S.; Oustadi, F.; Stephens, E. D.; Badv, M. Bacterial-Nanocellulose-Based Biointerfaces and Biomimetic Constructs for Blood-Contacting Medical Applications. *ACS Mater. Au* **2023**, *3*, 418−441.

(24) Nyakuma, B. B.; Wong, S.; Utume, L. N.; Abdullah, T. A. T.; Abba, M.; Oladokun, O.; Ivase, T. J. P.; Ogunbode, E. B. Comprehensive Characterisation of the Morphological, Thermal and Kinetic Degradation Properties of Gluconacetobacter xylinus synthesised Bacterial Nanocellulose. *J. Nat. Fibers* **2022**, *19*, 6255−6268.

(25) Ampomah-Wireko, M.; Luo, C.; Cao, Y.; Wang, H.; Nininahazwe, L.; Wu, C. Chemical probe of AHL modulators on quorum sensing in Gram-Negative Bacteria and as antiproliferative agents: A review. *Eur. J. Med. Chem.* **2021**, *226*, 113864.

(26) Thi, M. T. T.; Wibowo, D.; Rehm, B. H. A. Pseudomonas aeruginosa Biofilms. *Int. J. Mol. Sci.* **2020**, *21* (22), 8671.

(27) Sharma, I. M.; Petchiappan, A.; Chatterji, D. Quorum Sensing and biofilm formation in mycobacteria: role of c-di-GMP and methods to study this second messenger. *IUBMB Life* **2014**, *66* (12), 823−834.

(28) Zhang, T. Z.; Liu, L. P.; Ye, L.; Li, W. C.; Xin, B.; Xie, Y. Y.; Jia, S. R.; Wang, T. F.; Zhong, C. The production of bacterial cellulose in Gluconacetobacter xylinus regulated by luxR overexpression of quorum sensing system. *Appl. Microbiol. Biotechnol.* **2021**, *105*, 7801−7811.

(29) Liu, L. P.; Huang, L. H.; Ding, X. T.; Yan, L.; Jia, S. R.; Dai, Y. J.; Xie, Y. Y.; Zhong, C. Identification of quorum-sensing molecules of N-acyl-homoserine lactone in Gluconacetobacter strains by liquid chromatography-tandem mass spectrometry. *Molecules* **2019**, *24* (15), 2694.

(30) Yuen, J. D.; Walper, S. A.; Melde, B. J.; Daniele, M. A.; Stenger, D. A. Electrolyte-Sensing Transistor Decals Enabled by Ultrathin Microbial Nanocellulose. *Sci. Rep.* **2017**, *7*, 40867.

(31) Rudrappa, T.; Biedrzycki, M. L.; Bais, H. P. Causes and consequences of plant-associated biofilms. *FEMS Microbiol. Ecol.* **2008**, *64*, 153−664.

(32) Efthymiou, M.-N.; Tsouko, E.; Papagiannopoulos, A.; Athanasoulia, I.-G.; Georgiadou, M.; Pispas, S.; Briassoulis, D.; Tsironi, T.; Koutinas, A. Development of biodegradable films using sunflower protein isolates and bacterial nanocellulose as innovative food packaging materials for fresh fruit preservation. *Sci. Rep.* **2022**, *12*, 6935.

(33) Suryanto, H.; Muhajir, M.; Sutrisno, T. A.; Mudjiono; Zakia, N.; Yanuhar, U. The Mechanical Strength and Morphology of Bacterial Cellulose Films: The Effect of NaOH Concentration. *IOP Conf. Ser.: Mater. Sci. Eng.* **2019**, *515*, 012053.

(34) Dima, S.-O.; Panaitescu, D.-M.; Orban, C.; Ghiurea, M.; Doncea, S.-M.; Fierascu, R. C.; Nistor, C. L.; Alexandrescu, E.;

https://doi.org/10.1021/acsomega.3c10053
ACS Omega 2024, 9, 20003−20011

Nicolae, C.-A.; Trica, B.; Moraru, A.; Oancea, F. Bacterial Nanocellulose from Side-Streams of Kombucha Beverages Production: Preparation and Physical-Chemical Properties. *Polymers* **2017**, *9*, 374.

(35) Silverstein, R. M.; Bassler, G. C.; Morrill, T. C. *Spectrometric Identification of Organic Compounds*, 4th ed.; Wiley: New York, 1981.

(36) Soares, S.; Camino, G.; Levchik, S. Comparative study of the thermal decomposition of pure cellulose and pulp paper. *Polym. Degrad. Stab.* **1995**, *49*, 275−283.

(37) Hardy, B. J.; Sarko, A. Molecular dynamics simulations and diffraction-based analysis of the native cellulose fibre: structural modelling of the I-α and I-β phases and their interconversion. *Polymer* **1996**, *37* (10), 1833−1839.

https://doi.org/10.1021/acsomega.3c10053
ACS Omega 2024, 9, 20003−20011